JOURNAL OF SPACECRAFT AND ROCKETS
Vol. 38, No. 5, September–October 2001

X-33 Hypersonic Boundary-Layer Transition

Scott A. Berry,* Thomas J. Horvath,* Brian R. Hollis,† Rick A. Thompson,* and H. Harris Hamilton II*
NASA Langley Research Center, Hampton, Virginia 23681

Boundary-layer and aeroheating characteristics of several X-33 configurations have been experimentally examined in the NASA Langley Research Center 20-Inch Mach 6 Air Tunnel. Global surface heat transfer distributions, surface streamline patterns, and shock shapes were measured on 0.013-scale models at Mach 6 in air. Parametric variations include angles of attack of 20, 30, and 40 deg; Reynolds numbers based on model length of 9×10^5 to 6.6×10^6; and body-flap deflections of 0, 10, and 20 deg. The effects of discrete and distributed (in the form of wavy wall bowed panels) roughness on boundary-layer transition, which included trip height, size, location, and distribution, both on and off the windward centerline, were investigated. The discrete roughness results on centerline were used to provide a transition correlation for the X-33 flight vehicle that was applicable across the range of reentry angles of attack. The attachment line discrete roughness results were shown to be consistent with the centerline results because no increased sensitivity to roughness along the attachment line was identified. The effect of bowed panels was qualitatively shown to be less effective than the discrete trips; however, the distributed nature of the bowed panels affected a larger percent of the aft-body windward surface than a single discrete trip.

Nomenclature

H	=	enthalpy, BTU/lbm
h	=	heat transfer coefficient, $q/(H_{aw} - H_w)$ where $H_{aw} = H_{12}$, lbm/ft$^2 \cdot$ s
h_{FR}	=	reference coefficient using Fay–Riddell calculation to stagnation point of a scaled sphere
k	=	roughness element height, in.
L	=	reference length of model, 10.00 in.
M	=	Mach number
M_e	=	Mach number at edge of boundary layer
q	=	heat transfer rate, BTU/ft$^2 \cdot$ s
Re	=	unit Reynolds number, 1/ft
Re_L	=	Reynolds number based on body length
Re_θ	=	momentum thickness Reynolds number
W	=	roughness element width, in.
x	=	longitudinal distance from the nose, in.
y	=	lateral distance from the centerline, in.
α	=	model angle of attack, deg
δ	=	boundary-layer thickness, in.
δ_{BF}	=	body-flap deflection, deg

Introduction

THE X-33 is a technology demonstrator for a next-generation fully reusable launch vehicle (RLV) rocket that is intended to establish significant reductions in the cost of access to space.[1–3] As the prime contractor for the X-33, Lockheed Martin Skunkworks is building a slab-delta lifting body design[2] with canted fins, twin vertical tails, and two outboard body flaps located at the rear of the fuselage. A linear aerospike engine[4] is used to power the X-33, which is roughly a half-scale prototype of Lockheed's RLV design, the VentureStar. Figure 1 provides a comparison of the X-33 to the VentureStar and the current national launch system, the Space Shuttle Orbiter.

As part of the cooperative agreement, NASA Langley Research Center (LaRC) has been tasked with providing experimental boundary-layer transition and aeroheating data in support of X-33 aerothermodynamic development and design. To satisfy the objectives outlined in the task agreements, a combined experimental and computational approach was utilized. Results from early wind-tunnel heating measurements were compared to laminar and turbulent predictions and are reported in Ref. 5. Preliminary results associated with the effort to characterize the boundary layer on an early configuration of X-33 in flight are reported in Ref. 6. Since the time of these publications (early 1998), additional tests have been completed that supplemented the original database and accommodated design changes to the vehicle shape. The most current experimental and computational aeroheating results are presented in this report and two companion papers.[7,8]

This report presents an overview of the results to date of the investigation into boundary-layer transition for the X-33 configuration in LaRC facilities. The purpose of this investigation was to examine experimentally issues affecting boundary-layer transition and the effect of transition on the aeroheating characteristics of the X-33. Over a series of wind-tunnel entries in the NASA LaRC 20-Inch Mach 6 Air Tunnel, the smooth body transition patterns, the effect of discrete roughness on and off windward centerline, and the effect of distributed bowed panels have been examined. The primary test technique that was utilized during these tests was the thermographic phosphor technique,[9] which provides global surface heating images that can be used to assess the state of the boundary layer. Flow visualization techniques, in the form of oil flow to provide surface streamline information and schlieren to provide shock system details, were also used to supplement the heating data. Parametrics included in these tests were the effect of angle of attack (α of 20, 30, and 40 deg), unit Reynolds number (Re between 1×10^6 and 8×10^6/ft), body-flap deflections (δ_{BF} of 0, 10, and 20 deg), and roughness. The roughness tests included both discrete and distributed trip mechanisms. The discrete roughness parametrics (which included height, size, and location) were included in these tests to provide information to develop a roughness transition correlation for the X-33 vehicle and included results from both the centerline and attachment lines of the X-33. The distributed roughness was in the form of a wavy wall that simulates the expected metallic thermal protection system (TPS) panel bowing in flight due to temperature gradients across the panel. The current centerline results are from the latest X-33 configuration and will be compared to the earlier results presented in Ref. 6, which were obtained from a forebody model of an earlier configuration. Whereas the results presented in Ref. 6 were used to establish the transition correlation used for the X-33, the current results will validate the transition correlation for the newer configurations and extend the applicability of the correlation to off-centerline locations.

Received 23 July 1999; revision received 3 November 2000; accepted for publication 5 February 2001.

*Aerospace Technologist, Aerothermodynamics Branch, Aerodynamics, Aerothermodynamics, and Acoustics Competency.

†Aerospace Technologist, Aerothermodynamics Branch, Aerodynamics, Aerothermodynamics, and Acoustics Competency. Member AIAA.

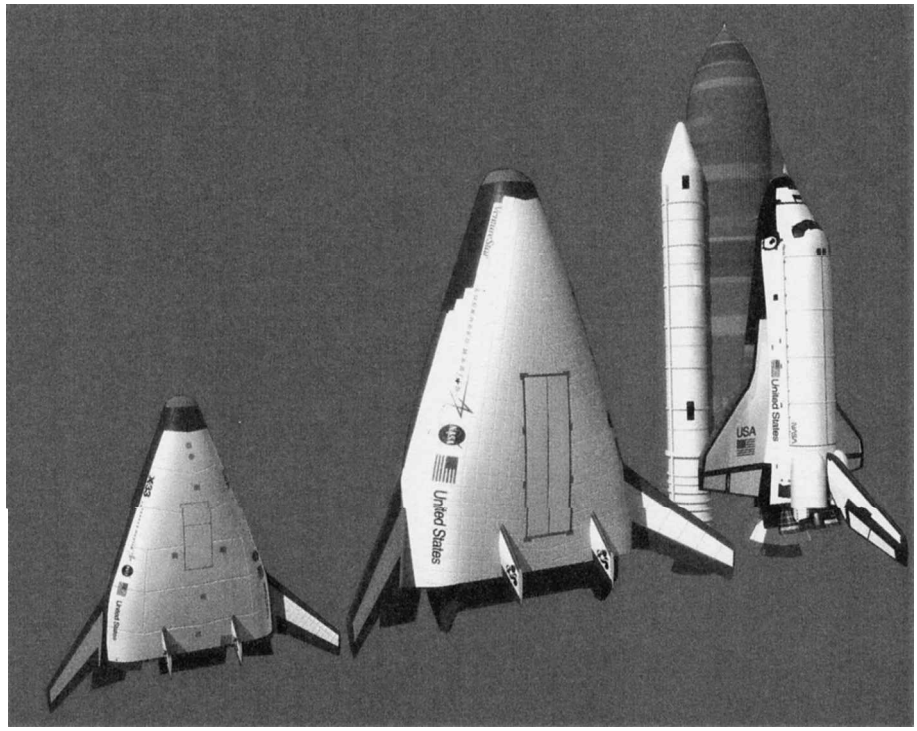

Fig. 1 Comparison of X-33 to proposed RLV and the Space Shuttle.

Boundary-Layer Transition in Flight

Boundary-layer transition, a historically difficult design issue for aerodynamicists, becomes even more critical for hypersonic flight due to the increased aeroheating effects.[10] TPS design is strongly influenced by the accurate prediction of when transition will occur.[6] Boundary-layer transition affects not only the maximum surface temperature (thus the TPS material selection[11]) through increased heating rates, but also the overall TPS mass (thickness) due to the increased total heat load.[12] There are numerous contributing factors that can influence the transition process, and a full description of all of them is beyond the scope of this paper. Stetson[13] provides a good practical survey of the key issues associated with the problem of hypersonic boundary-layer transition and provides an extensive reference list for those interested in an in-depth literature review.

As a current space transportation system, the Space Shuttle Orbiter is an obvious place to start when discussing hypersonic boundary-layer transition in flight. The shuttle design certainly was influenced by concerns regarding early transition, especially in regards to surface roughness effects.[14] An extensive wind-tunnel testing program was utilized during the shuttle evolution to understand and minimize the influence of roughness, predominately in the form of misalignments of the ceramic TPS tiles that produced local surface steps and gaps. Because modern computational methods were not yet available, the entire preflight shuttle aerothermodynamic database, including transition effects, was generated almost exclusively through the use of wind tunnels and simple extrapolation to flight techniques. The wind-tunnel derived transition criterion for flight that was developed was thought to be conservative due to the influence of noise that radiated from the turbulent tunnel walls of the facilities that were used.[15] The numerous shuttle reentries into the Earth's atmosphere represent a flight database[14] that essentially validates the simple and conservative methodology and assumptions that were utilized during the design. Indeed, for a majority of these flights, boundary-layer transition has been dominated by surface roughness[14] in the form of launch-induced damage and/or protruding gap fillers. The random nature of this roughness, unfortunately, allows for a wide range of free stream conditions for the onset of transition: Mach numbers between 6 and 18 and length Reynolds numbers between 2.5×10^6 and 1.3×10^7. This amount of scatter does little to induce confidence with regard to reliable prediction of hypersonic boundary-layer transition for future reentry vehicles. Perhaps, if the launched induced damage can be minimized and the protruding gap fillers eliminated for the next vehicle design, then more consistent transition results will be experienced in flight. Reduction of the uncertainty with regard to flight boundary-layer transition decreases unnecessary TPS margins and increases payload to orbit.

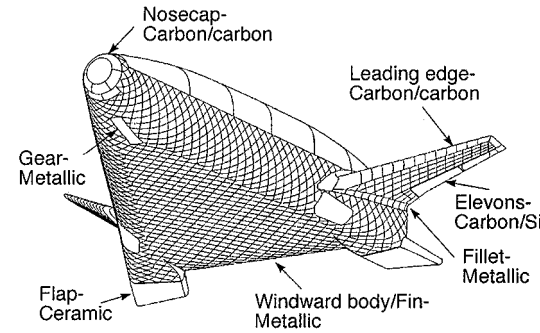

Fig. 2 X-33 windward surface TPS.

From the perspective of boundary-layer transition, the X-33 has some similarities to the Space Shuttle Orbiter. During reentry, both vehicles fly comparable trajectories and at angles of attack near 40 deg, which results in a moderately blunt flowfield that produces similar boundary-layer edge conditions on the windward surface (M_e between 1.5 and 2.0). Also, the TPS tiles that protect the X-33 windward surface are laid out in a diamond pattern similar to those on the shuttle (Fig. 2). The shuttle flight transition experience, therefore, provides the starting point with which to assess transition for the proposed X-33 flights.

Early in the shuttle program, the ceramic TPS was recognized to be relatively fragile, and studies were performed to suggest alternatives that offer more durability and operability without sacrificing weight.[12] During these studies, a metallic TPS was identified as the lightest system to provide a significant improvement in durability and operability for the shuttle program, but it was never implemented. A derivative of this metallic TPS[16,17] has been selected for use on the windward surface of the X-33, as shown in Fig. 2. This system is expected to offer improved durability against the random surface defects that continue to plague the shuttle. However, a detriment of this system is that it provides an additional type of surface roughness that has received very little attention over the years. During hypersonic flight, thermal gradients within the metallic TPS panels[18] will produce an outward bowing of the panels on the order of 0.25 in. The effect of this panel bowing on hypersonic

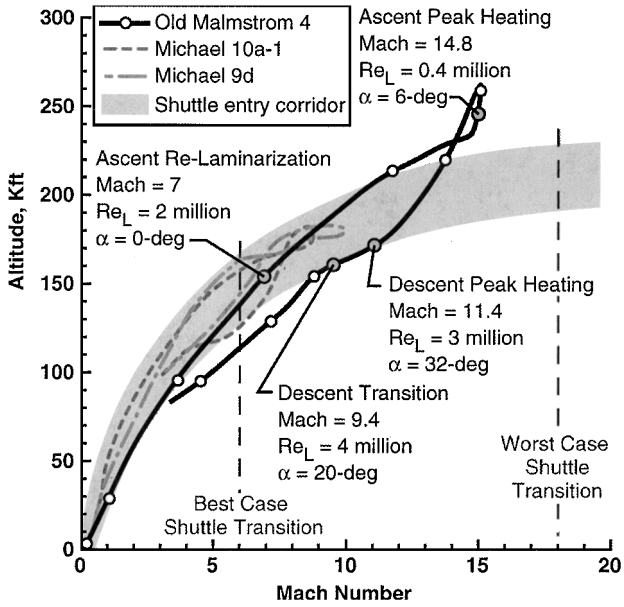

Fig. 3 Trajectory used for design of X-33 TPS.

boundary-layer transition is largely unknown and is part of the current investigation that will be described in this paper.

The suborbital trajectory used for the design of the TPS is shown in Fig. 3 and is designated as Old Malmstrom-4. This is a high-Mach-number trajectory that would land the X-33 at Malmstrom Air Force Base in Montana. The initial flights of the X-33 are lower-Mach-number trajectories to Michaels Air Force Base in Utah. (Preliminary Michaels trajectories are also shown for comparison.) Some select points (relevant to the TPS design) along the Old Malmstrom-4 trajectory are illustrated in Fig. 3. On ascent, the X-33 windward surface is assumed, for the purpose of the TPS design, to remain turbulent until $Re_L = 2 \times 10^6$. Thus, during peak heating on ascent, the windside boundary layer will be laminar, and the vehicle will be at a low angle of attack. As the top of the trajectory is reached, the vehicle pitches up to high angles of attack for most of the hypersonic descent. A second peak heating point occurs on descent at a Mach number near 11. Based on earlier results,[6] the X-33 boundary layer is expected to transition back to a turbulent state at a Mach number near 9. However, when viewed against the varied results experienced on the shuttle (the highest and lowest Mach number at transition shown in Fig. 3), the need to minimize known transition bypass mechanisms, which could force earlier transition (before the descent peak heating point), is evident.

Transition Prediction Approach

A series of wind-tunnel tests were performed to investigate the X-33 aeroheating and boundary-layer characteristics while changes to the configuration were tracked. Over 1100 tunnel runs from 16 entries in two facilities have been completed on four X-33 configurations since August 1996. The evolution of the X-33 configuration from the onset of Phase II has necessitated multiple entries into LaRC facilities to investigate the effects of outer mold line (OML) changes to X-33's aeroheating environment. The OML for the X-33 started with the original D-Loft concept, then the F-Loft Revision C (Rev-C), the F-Loft Revision F (Rev-F), and finally the F-Loft Revision G (Rev-G). These four configurations have been tested in LaRC facilities for both baseline aeroheating data (i.e., wide ranges of angle of attack, yaw, Reynolds number, body-flap deflection, etc.) and to investigate the effects of surface roughness (both discrete and distributed) and test technique (model scale, blade vs sting support, etc.). Additional details regarding the OML changes can be found in Ref. 7.

The testing sequence and model configurations tested are listed in Table 1 of Ref. 7. First, the effect of discrete roughness elements on the centerline of the D-Loft forebody was investigated in Test 6737. This test utilized the same approach that was used during an investigation into discrete roughness elements on the Shuttle Orbiter[19] that has shown good agreement with flight data.[20] These early test results are presented in Ref. 6. Then, during Test 6763, the effect of discrete roughness on the centerline of the Rev-F configuration was investigated for comparison to the earlier results. The effect of distributed roughness in the form of a wavy-wall surface (simulating bowed metallic TPS tiles) on Rev-F was investigated in Test 6769. The windward attachment line was examined during Test 6770 (Ref. 21) for comparison to trends found on the centerline. Finally, extended bowed panels on Rev-G were investigated during Test 6786. Collectively, these tests provide a systematic investigation of several different boundary-layer trip mechanisms while tracking the OML changes of the X-33 vehicle.

Experimental Methods

Test Facility

The present experiments were conducted in the NASA LaRC 20-Inch Mach 6 Air Tunnel. Miller[22] provides a detailed description of this hypersonic blowdown facility, which uses heated, dried, and filtered air as the test gas. Typical operating conditions for the tunnel are stagnation pressures ranging from 30 to 500 psia, stagnation temperatures from 760 to 940°R, and freestream unit Reynolds numbers from 5×10^5 to 8×10^6/ft. A two-dimensional, contoured nozzle is used to provide nominal freestream Mach numbers from 5.8 to 6.1. The test section is 20.5 by 20 in., and the nozzle throat is 0.399 by 20.5 in. A bottom-mounted model injection system can insert models from a sheltered position to the tunnel centerline in less than 0.5 s. Run times up to 15 min are possible with this facility, although for the current heat transfer and flow visualization tests, the model was exposed to the flow for only a few seconds. Flow conditions were determined from the measured reservoir pressure and temperature and the measured pitot pressure at the test section.

The 20-Inch Mach 6 Air Tunnel is considered a conventional facility with regard to freestream disturbance levels because it was built long before the quiet-tunnel[23] technology of the 1980s became available. Thus, freestream disturbances would be expected to influence the smooth-model transition data. In fact, Fig. 12 of Ref. 24 provides a comparison of recent shuttle transition data obtained in the 20-Inch Mach 6 Arnold Engineering Development Center (AEDC) Tunnel B, and flight and the differences noted are attributed to tunnel noise. The AEDC tests had the lowest values of Re_θ/M_e at transition and flight had the highest, which is the same conservative trend noted earlier during the shuttle aerothermodynamic database development. Thus, on the basis of transition results, the 20-Inch Mach 6 Air Tunnel would appear to be quieter than AEDC Tunnel B, albeit noisier than flight. However, the only recent attempt at quantifying the disturbance levels of this facility reported mass-flow fluctuations that were slightly higher (2–3% of mean)[25] than AEDC Tunnel B (1–2%)[26] and, of course, orders of magnitude higher than flight (0.01–0.02%).[26]

Test Techniques

Surface Heating

The rapid advances in image processing technology that have occurred in recent years have made digital optical measurement techniques practical in the wind tunnel. One such optical acquisition method is two-color, relative-intensity phosphor thermography, which is currently being applied to aeroheating tests in the hypersonic wind tunnels of NASA LaRC. Details of the phosphor thermography technique are provided in Refs. 9, 27, and 28, and Refs. 6, 19, and 29 are recent examples of the application of the technique to wind-tunnel testing. With this technique, ceramic wind-tunnel models are fabricated and coated with phosphors that fluoresce in two regions of the visible spectrum when illuminated with ultraviolet light. The fluorescence intensity is dependent on the amount of incident ultraviolet light and the local surface temperature of the phosphors. By acquiring fluorescence intensity images with a color video camera of an illuminated phosphor model exposed to flow in a wind tunnel, surface temperature mappings can be calculated on the portions of the model that are in the field of view of the camera. A temperature calibration of the system conducted before the study provides the look-up tables that are used to convert the ratio of the green and red intensity images to global temperature

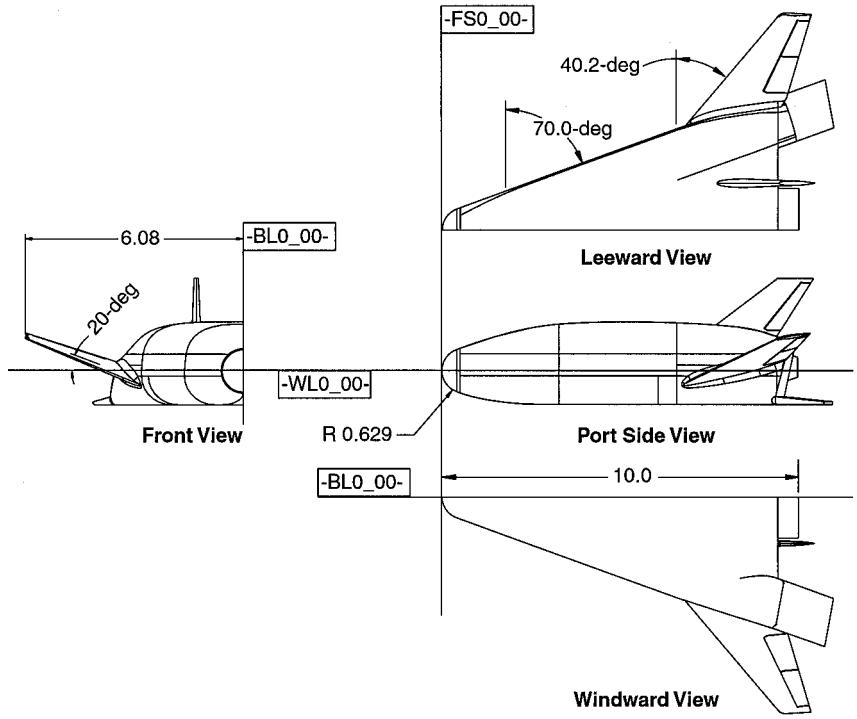

Fig. 4 X-33 Rev-F configuration.

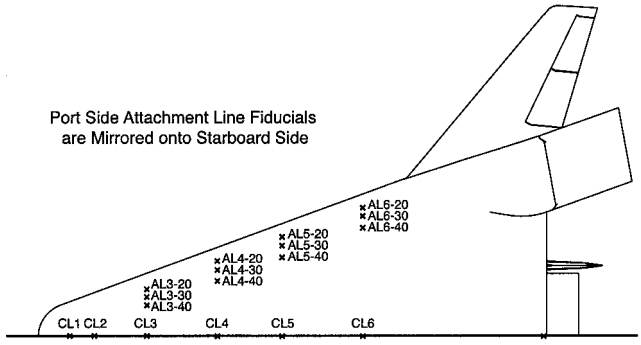

Fig. 5 Trip locations and fiducial marks.

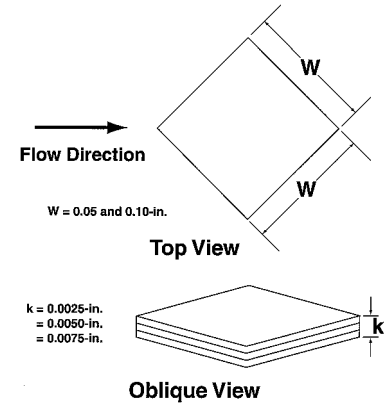

Fig. 6 Trips showing orientation, width, and height.

mappings. With temperature images acquired at different times in a wind-tunnel run, global heat transfer images are computed assuming one-dimensional heat conduction. The primary advantage of this technique is the global resolution of the quantitative heat transfer data. Such data can be used to identify the heating footprint of complex, three-dimensional flow phenomena (e.g., transition fronts, turbulent wedges, boundary-layer vortices, etc.) that are extremely difficult to resolve by discrete measurement techniques. Phosphor thermography is routinely used in the LaRC hypersonic facilities because quantitative global surface heating information is obtained from models that can be fabricated quickly (within a few weeks) and economically (cost an order of magnitude less than the thin-film technique). Recent comparisons of heat transfer measurements obtained from phosphor thermography to conventional thin-film resistance gauges measurements[30] and computational fluid dynamics predictions[5,6,29,31] have shown excellent agreement.

Flow Visualization

Flow visualization techniques, in the form of schlieren and oil flow, were used to complement the surface heating tests. The 20-Inch Mach 6 Air Tunnel is equipped with a pulsed white-light, Z-pattern, single-pass schlieren system with a field of view encompassing the entire 20-in. test core. Surface streamline patterns were obtained using the oil-flow technique. Both schlieren and oil-flow images were recorded with a high-resolution digital camera.

Model Description

The X-33 Rev-F model dimensions are shown in Fig. 4. A rapid prototyping technique was used to build resin stereolithography (SLA) models with various, detachable body flaps on both the port and starboard region of the base of the vehicle. The SLA model was then used with the various body flaps as a pattern to cast several ceramic model configurations. Additional details about model construction and the various configurations that were tested can be found in Ref. 21. The final step in the fabrication process is to apply fiducial marks along the body to assist in determining spatial locations accurately. The fiducial marks used for the present study are shown in Fig. 5.

The roughness elements used in this study were similar to those used in Refs. 6 and 19, which were fabricated to simulate a raised TPS tile and were cut from 0.0025-in.-thick tape made from polyimide film with a silicone adhesive. Presented in Fig. 6 is a typical discrete trip showing dimensions and orientation. Variations on the roughness heights k were obtained by stacking multiple layers of tape ($k = 0.0025, 0.0050$, and 0.0075 in.). Roughness elements fabricated from tape were applied to the various locations of interest on the model and could be easily removed without adversely affecting the phosphor coating. The polyimide tape was chosen through a trial and error process based on the ease of fabrication and application of

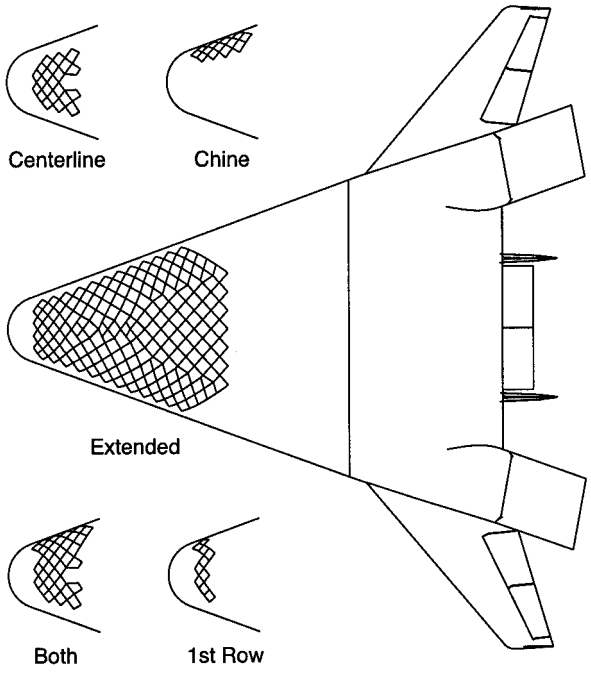

Fig. 7 Various bowed-panel configurations.

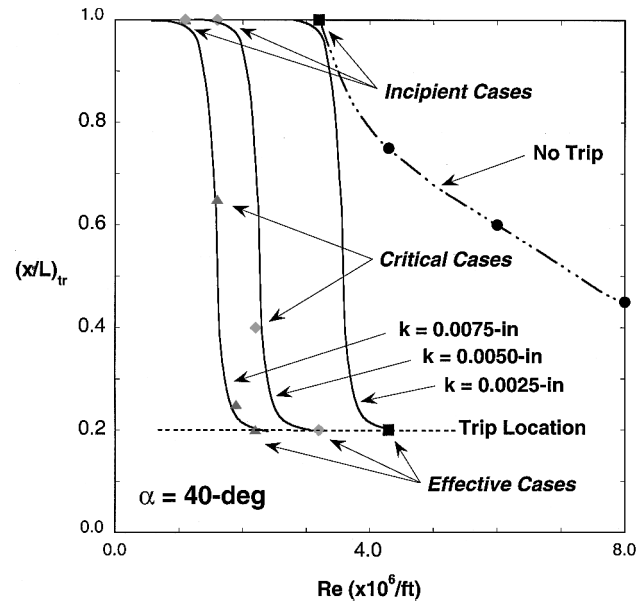

Fig. 8 Transition onset results on centerline for $\alpha = 40$ deg.

the roughness elements, as well as the durability of the material (and adhesive) to heat and shear stress loading. The roughness elements were placed directly over the various fiducial marks.

Bowed-panel models were also tested to simulate the effect of the wavy-wall windward surface that would be produced by the temperature gradients within the metallic TPS panels. The five configurations tested are shown in Fig. 7. Each configuration was constructed with nominal bow heights of 0.002, 0.004, 0.006, and 0.008 in. Two models of each configuration were built and tested to provide a statistical database with which to assess the results. A geometric scaling of the estimated in-flight bow height of 0.25 in. would be on the order of 0.003 in.

Test Conditions

The NASA LaRC 20-Inch Mach 6 Air Tunnel provides a freestream unit Reynolds number variation from 5×10^5 to 8×10^6 /ft. For a 0.0132-scale model, this range corresponds to a length Reynolds number from approximately 4.1×10^5 to 6.7×10^6. For the baseline data, the model angle of attack α was varied from 20 to 40 deg in 10-deg increments, and the sideslip was maintained at 0 deg for all of the runs presented herein. For each model configuration, the unit Reynolds number Re was varied between 1×10^6 and 8×10^6 /ft to obtain the smooth baseline data for comparison to the tripped data. For testing with trips, the same unit Reynolds number range was used with the roughness element firmly applied to the location of interest to determine the incipient, critical, and effective Reynolds numbers. Note that the terminology used here is similar to the definitions of Bertin et al.,[32] except that here the terms are a function of unit Reynolds number instead of trip height. Van Driest and Blumer[33] and Boudreau[34] both discuss trip effectiveness as a function of unit Reynolds numbers, but without the use of these specific terms. Whereas Boudreau defined effectiveness based on the end of transition, here transition onset is used (in the tradition of Bertin et al.[32]). For the present study, therefore, the incipient Reynolds number is defined as the maximum Re at which laminar flow was maintained behind the trip. The Re where significant nonlaminar flow first appears downstream of the roughness element identifies the critical value. Finally, the minimum Re where the transition front is fixed at the roughness element identifies the effective value. Generally, the unit Reynolds number increment from run to run was on the order of 5×10^5 /ft. Therefore, due to this increment, the incipient, critical, and effective values of the Re would be identified within three runs, typically. For example, Fig. 8 illustrates transition onset results as a function of Re for the X-33 at $\alpha = 40$ deg for three different trip heights as compared to the smooth model results. Clearly, a large movement in transition onset location is obtained for tripped cases by relatively small increases in Reynolds number.

Data Reduction

Heating rates were calculated from the global surface temperature measurements using one-dimensional semi-infinite solid heat-conduction equations.[9,28] The phosphor system measurement error is believed to be better than $\pm 8\%$, with overall experimental uncertainty of $\pm 15\%$ (Ref. 9). Heating distributions are presented in terms of the ratio of heat transfer coefficient h/h_{FR}, where h_{FR} corresponds to the Fay and Riddell[35] stagnation-point heating to a sphere with radius 0.629 in. (the nose radius of the Rev-F configuration scaled to the model size). Repeatability of the centerline heat transfer distributions was found to be generally better than $\pm 4\%$.

Computational Methods

Computational predictions for comparison to the wind-tunnel aeroheating test results were generated at select angles of attack and test conditions using the GASP code[36] and the LATCH code.[37] The GASP computations were used to assess the state of the boundary layer for the wind-tunnel cases, whereas the LATCH results were used to generate the boundary-layer transition correlation parameters. GASP is a three-dimensional, finite volume Navier–Stokes solver that incorporates numerous options for flux-splitting methods, thermochemical and turbulence models, and time-integration schemes. A perfect gas air model was employed and both fully laminar and fully turbulent solutions were obtained. Further details regarding the GASP computations can be found in Ref. 8. The LATCH code is an approximate three-dimensional heating code based on the axisymmetric analog for general three-dimensional boundary layers. An integral heating method is used to compute the heating rates along three-dimensional inviscid streamlines. The inviscid streamlines were supplied using an inviscid version of the LAURA code. Further details regarding the LATCH computations can be found in Ref. 5.

Discussion of Results

Smooth Body

The effect of angle of attack on smooth-body boundary-layer transition is shown in Fig. 9. (Note that the global heating images provided in this report are shown without the color bar scale because they are intended to show transition front locations only. Quantitative comparison of the data to computational results is provided in subsequent extracted heating profiles.) These heating images were obtained on a Rev-F model with a body-flap deflection of 20 deg

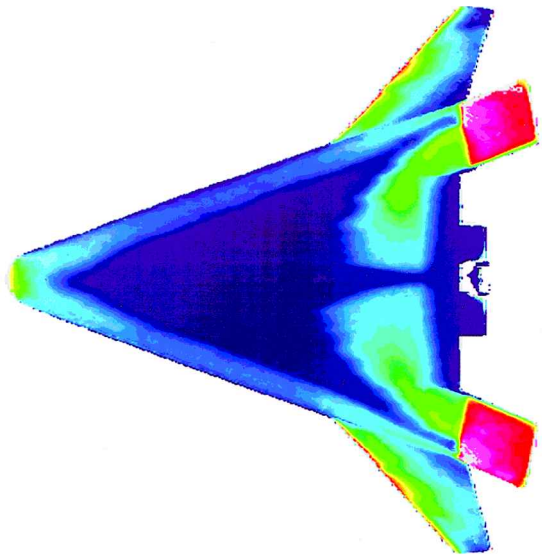

a) $\alpha = 20$ deg

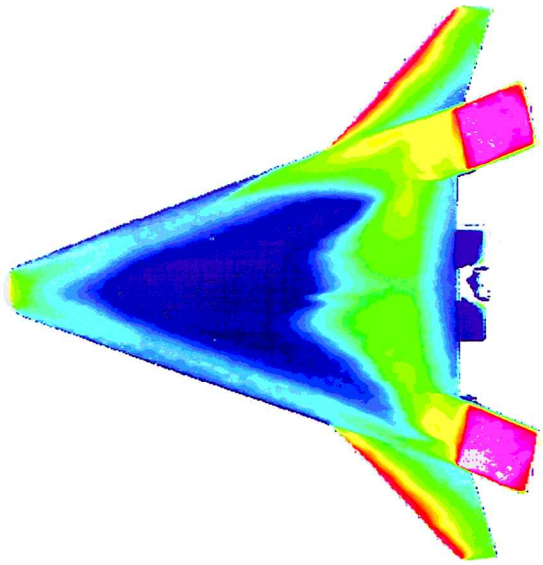

b) $\alpha = 30$ deg

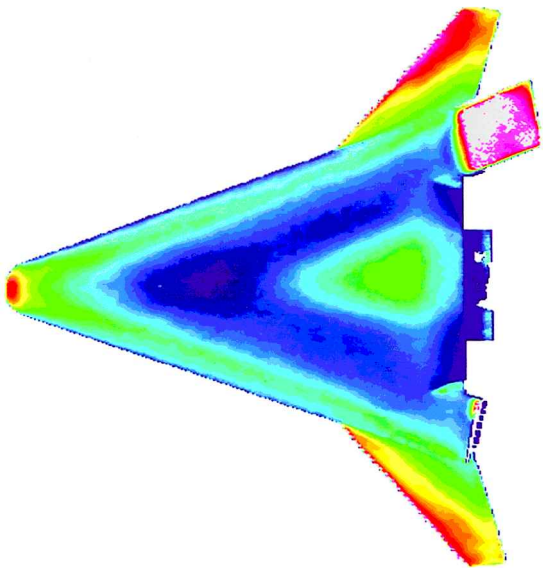

c) $\alpha = 40$ deg

Fig. 9 Effect of α on smooth body transition patterns at $Re = 7.8 \times 10^6$ /ft and $\delta_{BF} = 20$ deg.

for a unit Reynolds number of approximately 8×10^6 /ft. As will be discussed in more detail subsequently, the increased heating region toward the aft end of the model identifies the onset of boundary-layer transition. Note the changing shape of the transition front as α increases. Figure 9a ($\alpha = 20$ deg) shows two transition lobes separated by a laminar region on centerline. At $\alpha = 30$ deg (Fig. 9b) the two lobes have begun to merge on centerline. For $\alpha = 40$ deg (Fig. 9c), a single parabolic transition front symmetric about the centerline appears. This behavior was first noted on an early X-33 configuration[6] and appears to be related to changes in the direction of the forebody streamlines.[7] At the lower angles of attack, the forebody generates surface streamlines that curve predominately in toward the centerline (inflow). This inflow promotes a thickening of the boundary layer on centerline that tends to delay transition. The highly curved streamlines on the outboard regions of the forebody would likely induce crossflow instabilities that feed in from the chines. At the higher angles of attack, the surface streamlines tend to straighten out or even reverse direction to a slight outflow condition. For these cases, boundary-layer transition along the forebody centerline is likely to be dominated by the flow from the nose region.

The effect of varying Reynolds number on extracted heat transfer profiles along the model centerline for each α is shown in Fig. 10 with comparison of the smooth-body results to tripped cases and to laminar and turbulent heating predictions from Ref. 8. For the smooth-body data, the heating profiles are seen to agree (within the experimental uncertainty) with the laminar GASP predictions until the onset of natural transition occurs on the aft end of the model at higher Reynolds numbers. The forward progression of the transition onset point with increasing unit Reynolds number is the farthest forward at $\alpha = 40$ deg (Fig. 10c). The tripped cases were selected for comparison with the turbulent predictions and are also observed to agree within the experimental uncertainty. The LATCH results, on the other hand, are higher than the experimental data along the centerline, outside the experimental uncertainty, and the disparity increases with decreasing angle of attack. As shown in the axial comparisons of Ref. 8, this disagreement between LATCH and the experimental data, however, is mostly isolated to the centerline. Outboard of centerline, the experimental high heating region on the chine is matched by both the GASP and LATCH calculations. Moving inboard, the agreement is still good until the centerline is reached, and the drop in experimental heating is captured by the GASP results. The LATCH results have plateaued at the higher level. Because the disagreement between the experimental data and LATCH worsens as the angle of attack is decreased, perhaps LATCH is not accounting for the buildup of the boundary layer on centerline that results from inflow of the surface streamlines. Although the LATCH heating calculations are not in close agreement with the experimental results along the centerline, the effect of this overprediction should not strongly affect the boundary-layer edge parameters used for the present correlation. Reference 19 reported a similar disagreement with comparison to heating predictions, which resulted in only a 1–2% error in boundary-layer edge calculations.

Discrete Roughness Along Model Centerline

As an example of the many discrete trip results that were obtained, the effect of a 0.005-in. discrete trip at location CL3 is shown in Fig. 11 for each α. These heating images were obtained on a Rev-F model with a δ_{BF} of 0 deg. Figure 11a illustrates that for $\alpha = 20$ deg and $Re = 4.2 \times 10^6$ /ft, the 0.005 in. trip at CL3 just begins to have an effect on the downstream boundary layer. This case is considered critical because the turbulent wedge is not fixed at the trip (and at the next lower unit Reynolds number, laminar flow was maintained behind the trip). For $\alpha = 30$ deg and $Re = 4.2 \times 10^6$ /ft (Fig. 11b), the trip now produces a turbulent wedge directly behind the trip. This case would be classified as effective. As the angle of attack is increased to 40 deg (Fig. 11c), the trip is now an effective trip at $Re = 3.1 \times 10^6$ /ft.

From the sample results presented in Fig. 11, one might be tempted to conclude that the X-33 vehicle would be more sensitive to discrete trips at higher angles of attack. This conclusion is not supported when all of the results for discrete trips are used, in

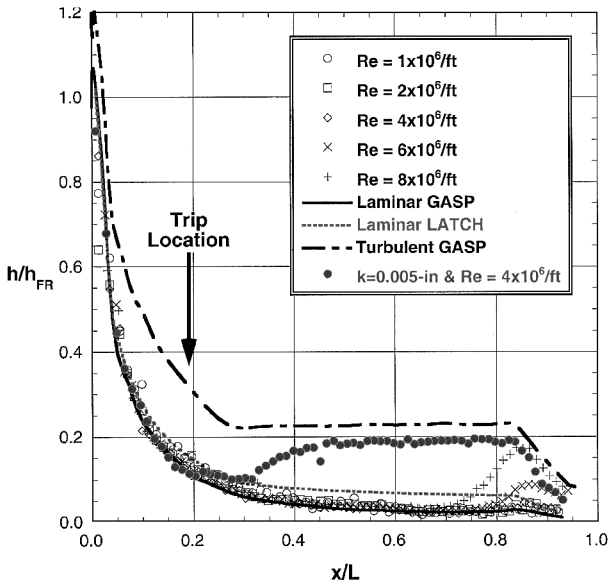

a) $\alpha = 20$ deg

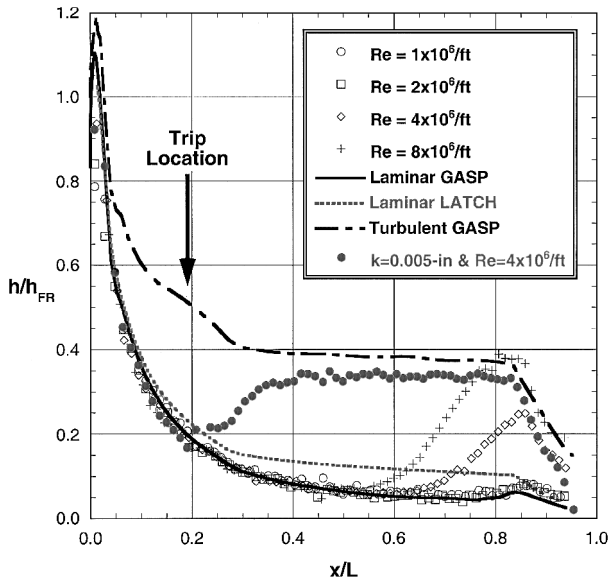

b) $\alpha = 30$ deg

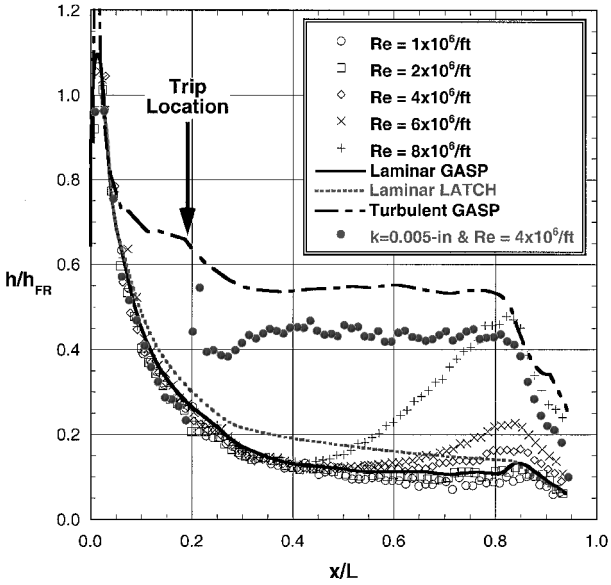

c) $\alpha = 40$ deg

Fig. 10 Reynolds number effect at each α for smooth and tripped cases with comparison to prediction.

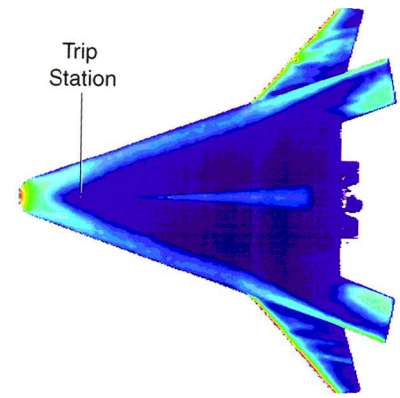

a) $\alpha = 20$ deg and $Re = 4.2 \times 10^6$ /ft

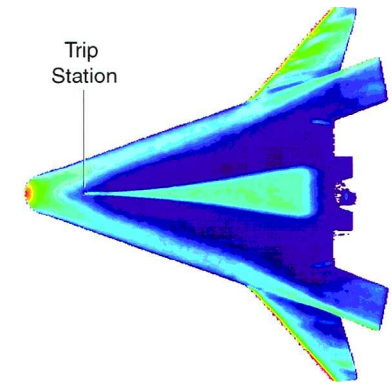

b) $\alpha = 30$ deg and $Re = 4.2 \times 10^6$ /ft

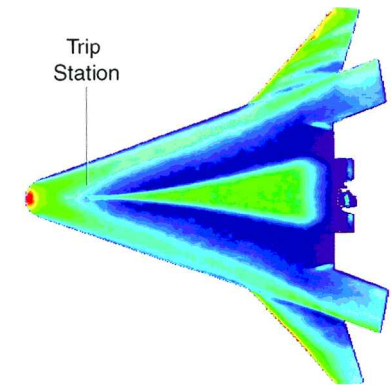

c) $\alpha = 40$ deg and $Re = 3.1 \times 10^6$ /ft

Fig. 11 Effect of 0.005-in. discrete trip at CL3 for $\delta_{BF} = 0$ deg.

conjunction with the boundary-layer calculations, to generate a Re_θ/M_e vs k/δ correlation. Figure 12 provides the results of this correlation for all of the discrete trip results along the model centerline for angles of attack of 20, 30, and 40 deg. (A similar figure is reported in Ref. 6 based on data from an early D-Loft forebody model.) The simple curves shown conservatively approximate the well-behaved patterns of incipient and effective transition data.

The experimental transition results presented thus far have already supported the X-33 program. A value of $Re_\theta/M_e = 250$ at $x/L = 0.8$ on the windward centerline was chosen as the transition criterion based on a conservative view of the smooth-body and discrete centerline roughness results, as well as experience from the shuttle.[6] The simplicity of this result has allowed development of a numerical tool that predicts when transition will occur on the windward centerline for a given altitude, velocity, and angle-of-attack condition. The transition tool is based on a database of numerical simulations that cover the range of altitudes, velocities, and angles of attack expected in flight. The coupling of this tool with trajectory simulations enables modifications of the flight profile to be made to ensure TPS design constraints are not exceeded. Further details

regarding the development and utility of this transition function can be found in Ref. 6. Also, the discrete roughness data have been used to estimate the allowable roughness heights for the flight vehicle. Based on the incipient curve of Fig. 12, the flight criterion for transition onset ($Re_\theta/M_e = 250$) corresponds to an allowable k/δ of 0.2. With this value of k/δ and the calculated boundary-layer thickness at the point on the trajectory that corresponds to the onset of transition, the allowable roughness heights over the windward surface are inferred and reported in Ref. 6.

Discrete Roughness Off-Centerline

Once the roughness criterion was established for the X-33 centerline, the next step was to verify if the discrete centerline criterion was applicable to off-centerline locations as well. The attachment line has been suggested by some[38] to be one of the most important locations for increased sensitivity to surface roughness. A program was initiated to investigate the effect of disturbances along the attachment lines for the X-33. The LATCH[5] code was used to predict the location of the attachment lines for angles of attack of 20, 30, and 40 deg (with nominal tunnel flow conditions as inputs). These attachment lines were used to locate the fiducial marks on the model for placement of the individual roughness elements (note that the attachment line fiducials correspond in terms of x/L to the same centerline locations used for the preceding discussion). These fiducial mark locations are shown in Fig. 6. Both the port and starboard side of the windward surface was marked to examine flow symmetry. The experimental attachment lines were determined using the oil flow technique and were found to correspond to prediction. For example, in Fig. 13, the attachment line is found by locating the surface streamline that curves neither to the leeside nor toward the centerline and that can be seen for this 30-deg example to coincide with the middle fiducial marks ($\alpha = 30$ deg). Similar results were obtained for angles of attack of 20 and 40 deg.

The roughness effects were examined only after the attachment line fiducial locations were verified for each angle of attack. Examples of typical heating images, which illustrate flow symmetry, and extracted heating profiles along the attachment line are provided in Figs. 14 and 15. For $\alpha = 30$ deg (Fig. 14), 0.005-in. trips at station 4 (on the port and starboard attachment lines, as well as the centerline) appear to be effective at $Re = 3.1 \times 10^6$/ft on the attachment lines, but not along the centerline. Similar results are shown in Fig. 15 for $\alpha = 40$ deg. Again, one might be tempted to draw the conclusion from these images that attachment lines appear to be more sensitive to discrete trips than the centerline. However, this conclusion is also not supported when the attachment line discrete trip results are compared to the results for the centerline discrete trip correlation (Fig. 12). This comparison is shown in Fig. 16 (a few data points have been omitted for clarity). The diagonal lines correspond to each Reynolds number sweep for a given trip configuration. At low unit Reynolds number there is no effect of the trip (open circle for laminar). As the unit Reynolds number increases, the first effects are noticed (open square for transitional). Finally, fully turbulent conditions up to the trip are seen (filled square). In general, these off-centerline results show very good agreement with the earlier centerline data. Thus, the transition correlation that was published earlier for the centerline data[6] has now been shown to be applicable to off-centerline locations as well. This study did not show any evidence of a higher sensitivity to roughness elements placed along the attachment line. However, the images of Figs. 14 and 15 illustrate that disturbances along the attachment lines will have a bigger impact on the aft body than trips on centerline.

Poll[38] has proposed a transition onset criterion for attachment line boundary-layer transition. This transition criterion is not the easiest to use because it is based on a velocity gradient term that is not typically calculated with boundary-layer or Navier–Stokes codes. In an effort to compare Poll's criterion with the current discrete roughness results, data from Poll's swept cylinder attachment-line curve has been recast in terms of the current X-33 results. As discussed earlier, the LATCH code has been used to compute heating and boundary-layer edge parameters on the X-33 vehicle. Hollis et al.[8] has shown that the LATCH computations are in very good agreement with Navier–Stokes calculations in the chine region where the attachment lines are located. For the flow conditions of interest, the LATCH code can be used to compute the approximate three-dimensional momentum thickness Reynolds number Re_θ on the attachment line along with all other boundary-layer edge properties. This information can then be used as input to a swept cylinder boundary-layer code[39] to compute Re_θ for an equivalent swept cylinder. The only unknown in this computation is the velocity gradient normal to the

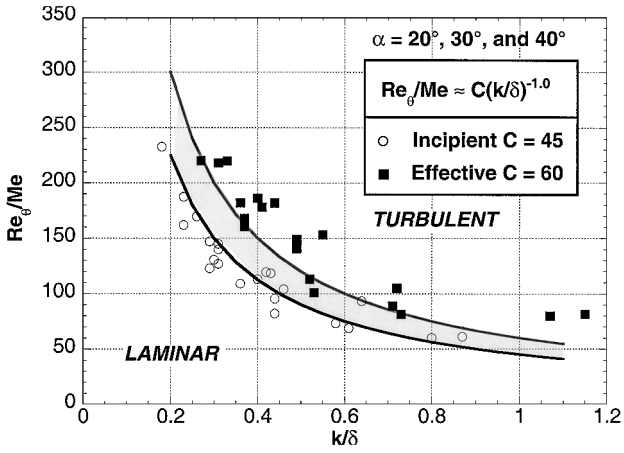

Fig. 12 Results of X-33 windward centerline transition correlation.

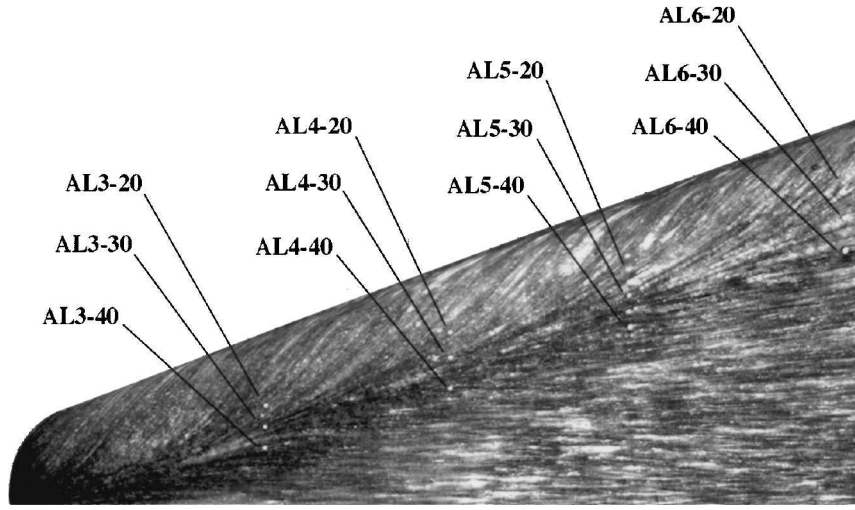

Fig. 13 Surface streamlines showing attachment line location for $\alpha = 30$ deg.

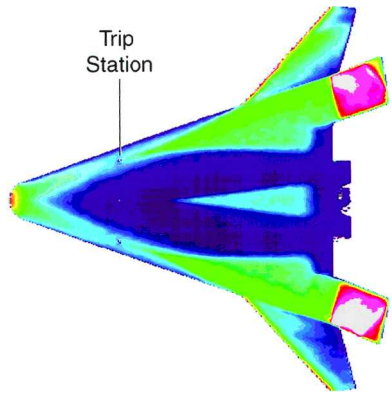

a) Heating image showing transition front for $Re = 3.1 \times 10^6$ /ft, and $\delta_{BF} = 20$ deg

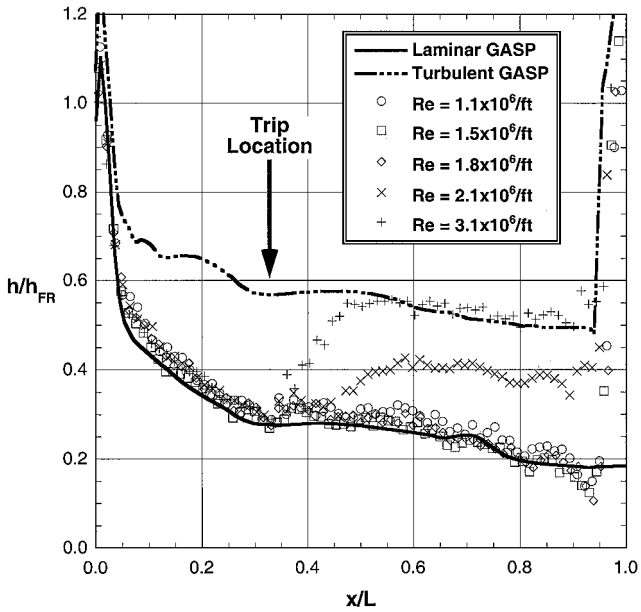

b) Reynolds number effect on heating along chine with comparison to predictions

Fig. 14 Effect of 0.005-in. discrete trips at AL4-30 for $\alpha = 30$ deg.

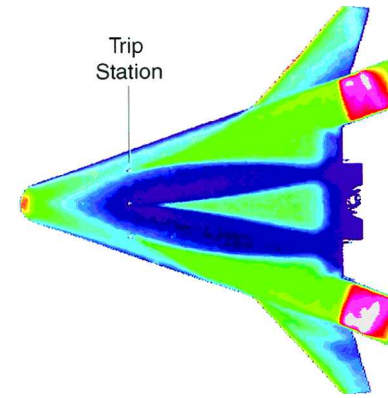

a) Heating image showing transition front for $Re = 3.1 \times 10^6$ /ft and $\delta_{BF} = 20$ deg

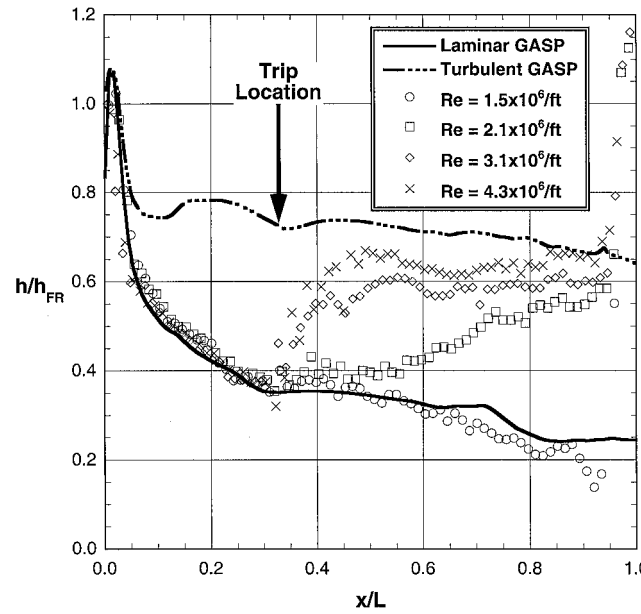

b) Reynolds number effect on heating along chine with comparison to predictions

Fig. 15 Effect of 0.005-in. discrete trips at AL4-40 for $\alpha = 40$ deg.

attachment line. By iterating on this velocity gradient, the momentum thickness Reynolds number from the swept cylinder calculation can be matched to the approximate three-dimensional momentum thickness Reynolds number computed by LATCH. This yields an equivalent velocity gradient along the attachment line, which is the last unknown required to compute Poll's transition parameters.[38] Once the velocity gradient is known, the current flow conditions and the attachment line criterion curve (Fig. 2 in Ref. 38) can be used to determine Poll's roughness heights k that cause boundary-layer transition onset. Finally, using k based on Poll's curve and Re_θ / M_e and δ from LATCH, the attachment line criterion has been recast in terms of the discrete roughness parameters for the X-33, as shown in Fig. 17. Roughly 45 datapoints were computed (corresponding to three angles of attack, five Reynolds numbers, and three axial locations along the attachment line) as shown by the filled-in symbols of Fig. 17. Presented in this manner, the original Poll attachment-line criterion for transition onset appears less conservative than the current incipient curve developed for X-33.

Distributed Roughness

The final transition issue that was investigated for the X-33 was the effect of the bowed metallic TPS panels. Five configurations were selected for testing that placed the location and extent of the bowed panels at various stations on the windward forebody, as shown in Fig. 8. The maximum bow height over the windward surface in flight is expected to be on the order of from 0.15 to 0.30 in. Based on the scale of the model (1.32%), this corresponds

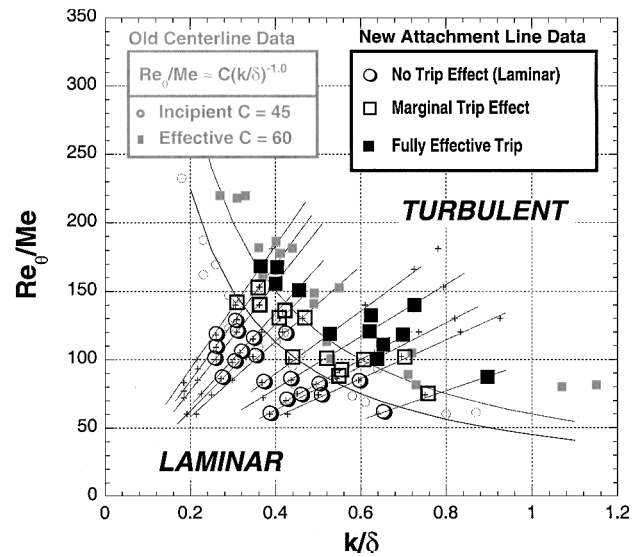

Fig. 16 Attachment line results compared to preceding centerline discrete roughness correlation.

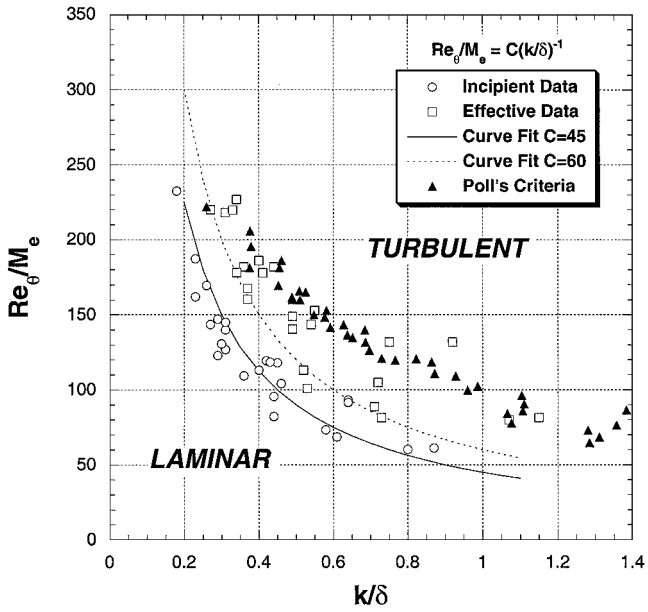

Fig. 17 Comparison of X-33 roughness transition correlation to Poll's criteria.[38]

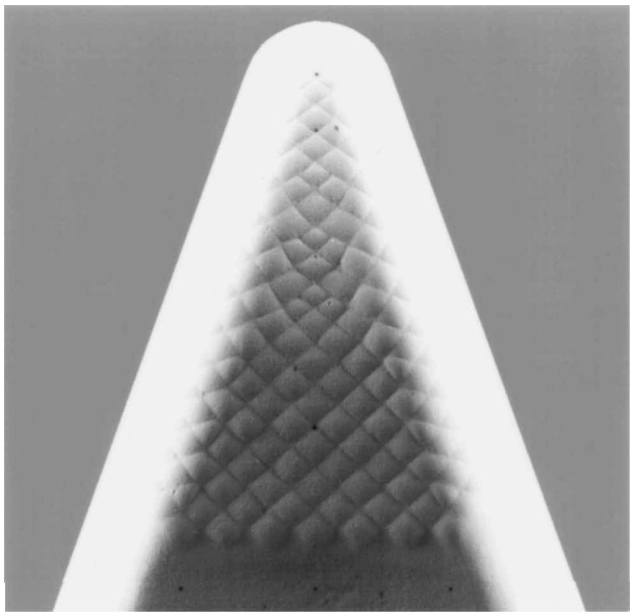

Fig. 18 Photograph of $k = 0.008$ in. extended bowed-panels model.

to geometrically scaled bow heights on the order of from 0.002 to 0.004 in. Additional heights of from 0.006 and 0.008 in. were also selected to provide an adequate range of wall waviness. For all configurations and heights, a primary and secondary model was built and tested to provide repeatability data.

As an example of the many bowed-panels configurations that were tested, a photograph of the 0.008-in. extended bowed-panels model is shown in Fig. 18. The effect of this extreme case on the surface streamlines for $\alpha = 40$ deg and $Re = 2 \times 10^6$ /ft is shown in Fig. 19. The surface streamlines are seen to serpentine around each bowed panel. The corresponding schlieren image, shown in Fig. 20, indicates that this level of bowing is sufficient enough to generate a series of shocklets that are seen to reflect off of the bow shock. Not surprisingly, this amount of flowfield disturbance is enough to affect the boundary layer, as shown in the corresponding heating image of Fig. 21.

The example selected is an extreme case that has over twice as much bowing geometrically than is expected in flight. However, the forward movement of transition for this extreme case can be seen to be still less than the effective discrete trip case shown in

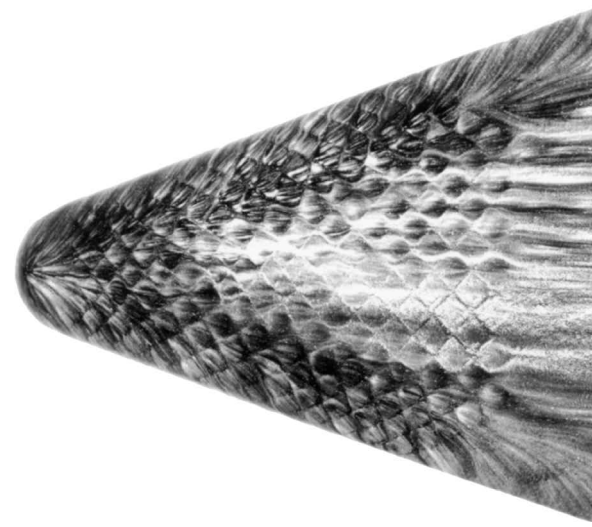

Fig. 19 Surface streamlines on $k = 0.008$ in. extended bowed panels for $\alpha = 40$ deg and $Re = 2 \times 10^6$ /ft.

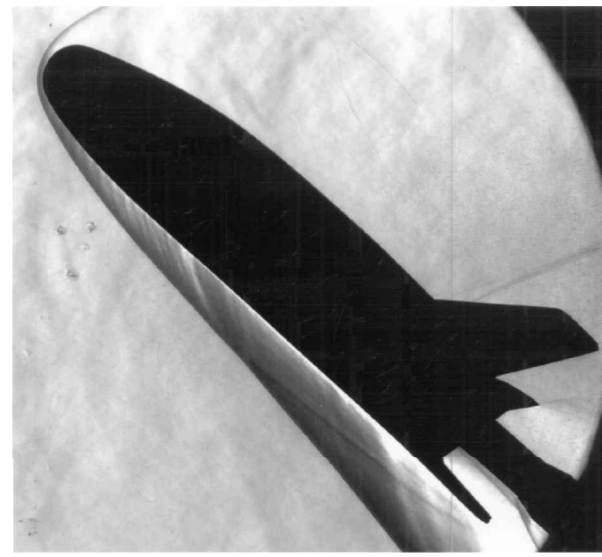

Fig. 20 Effect of $k = 0.008$ in. extended bowed panels on bow shock for $\alpha = 40$ deg, $Re = 4 \times 10^6$ /ft, and $\delta_{BF} = 0$ deg.

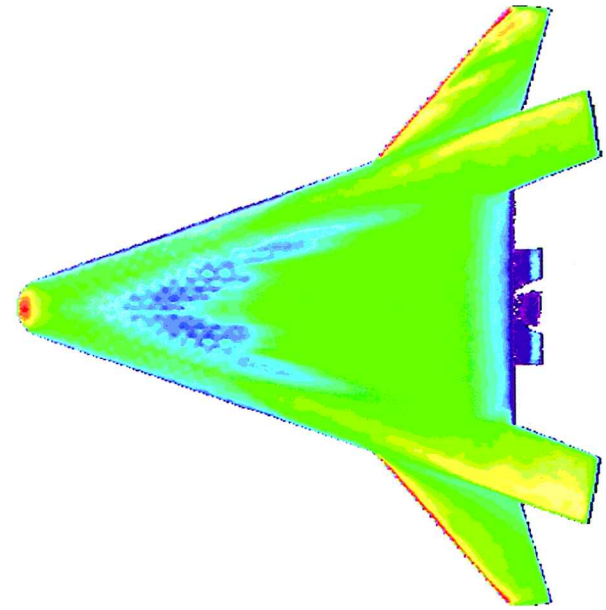

Fig. 21 Effect of $k = 0.008$ in. extended bowed panels on heating for $\alpha = 40$ deg, $Re = 4 \times 10^6$ /ft, and $\delta_{BF} = 0$ deg.

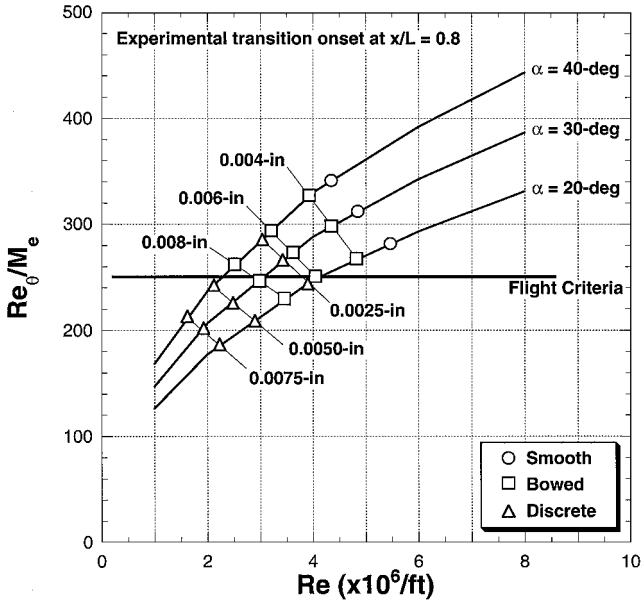

Fig. 22 Comparison of wind-tunnel results of smooth, bowed, and discrete trip tests to flight criteria.

Fig. 11c, which corresponds to a smaller disturbance at a lower Reynolds number. To illustrate this point further, Fig. 22 is a simplified comparison of the X-33 flight criterion as applied to the wind-tunnel transition onset results for smooth, discrete, and bowed panels. Figure 22 consists of curves of the calculated values of Re_θ/M_e at $x/L = 0.8$ on centerline as a function of unit Reynolds number for all three angles of attack. The data points shown on these curves are the experimental observance of the first nonlaminar heating levels at the $x/L = 0.8$ station for the smooth, discrete, and bowed-panels data for each α. The experimental points represent the general trends for many runs, including repeat runs on primary and backup models, as well as on multiple configurations. For the discrete data, the experimental points represent the various trip locations along the centerline. The flight criterion of $Re_\theta/M_e = 250$ is shown to conservatively cover the smooth model transition onset results for all reentry α. Also, the bowed panel results are also mostly covered by the built-in conservatism. On the other hand, the discrete results are shown to be more effective than the bowed panels at forcing transition onset at $x/L = 0.8$.

Conclusions

A series of experimental investigations into several issues affecting boundary-layer transition on the X-33 vehicle has been performed in the NASA LaRC 20-Inch Mach 6 Air Tunnel. These investigations examined natural transition on a smooth body, transition due to discrete roughness on the centerline and attachment lines, and transition due to distributed roughness in the form of wavy-wall bowed panels. Phosphor thermography was used to provide global heating images of the windward surface and assess the state of the boundary layer. The size and location of the various roughness mechanisms were systematically altered, and the subsequent response of the boundary layer was captured in the surface heating images. The experimental heating levels were compared to predictions to determine the onset location of transition and fully turbulent flow. Flowfield parameters from a boundary-layer code were used for analysis of transition correlations.

The smooth-body results indicate a significant change in the transition pattern as the reentry angle of attack changes from 20 to 40 deg. At lower α, a two-lobed transition front, indicative of cross-flow transition from the chine regions, is evident, whereas at higher α, a single parabolic transition front is centered about the model centerline. The discrete roughness results on centerline were used to provide a transition correlation for the X-33 flight vehicle that was applicable across the range of reentry angles of attack. To estimate the onset of transition in flight, the value of $Re_\theta/M_e = 250$ at $x/L = 0.8$ on the windward centerline was selected. This corresponded to a $k/\delta = 0.2$ from the discrete correlation curve, which was used to estimate the allowable roughness for the flight vehicle. The attachment line discrete roughness results were shown to be consistent with the centerline results because no increased sensitivity to roughness along the attachment line was identified. However, the effective trips on the attachment lines were shown to affect a larger percent of the aft body than trips on centerline. Finally, the effect of bowed panels was qualitatively shown to be less effective than the discrete trips, however, the distributed nature of the bowed panels affected a larger percent of the aft body than a single discrete trip.

References

[1]Bekey, I., Powell, R., and Austin, R., "NASA Studies Access to Space," *Aerospace America*, Vol. 32, No. 5, 1994, pp. 38–43.

[2]Cook, S. A., "X-33 Reusable Launch Vehicle Structural Technologies," AIAA Paper 96-4563, Nov. 1996.

[3]Freeman, D. C., Jr., Talay, T. A., and Austin, R. E., "Reusable Launch Vehicle Technology Program," International Astronautial Federation, IAF Paper 96-V.4.01, Oct. 1996.

[4]Baumgartner, R. I., and Elvin, J. D., "Lifting Body: An Innovative Reusable Launch Vehicle Concept," AIAA Paper 95-3531, Sept. 1995.

[5]Hamilton, H., Berry, S., Horvath, T., and Weilmuenster, J., "Computational/Experimental Aeroheating Predictions for X-33 Phase II Vehicle," AIAA Paper 98-0869, Jan. 1998.

[6]Thompson, R. A., Hamilton, H. H., Berry, S. A., and Horvath, T. J., "Hypersonic Boundary-Layer Transition for X-33 Phase II Vehicle," AIAA Paper 98-0867, Jan. 1998.

[7]Horvath, T. J., Berry, S. A., Hollis, B. R., Liechty, D. S., Hamilton, H. H., II, and Merski, N. R., "X-33 Experimental Aeroheating at Mach 6 Using Phosphor Thermography," *Journal of Spacecraft and Rockets*, Vol. 38, No. 5, 2001, pp. 634–645; also AIAA Paper 99-3558, June 1999.

[8]Hollis, B. R., Horvath, T. J., Berry, S. A., Hamilton, H. H., II, Thompson, R. A., and Alter, S. J., "X-33 Computational Aeroheating Predictions and Comparison with Experimental Data," *Journal of Spacecraft and Rockets*, Vol. 38, No. 5, 2001, pp. 658–669; also AIAA Paper 99-3559, June 1999.

[9]Merski, N. R., "Reduction and Analysis of Phosphor Thermography Data with IHEAT Software Package," *Journal of Spacecraft and Rockets*, Vol. 36, No. 2, 1999, pp. 160–170; also AIAA Paper 98-0712, Jan. 1998.

[10]Anderson, J. D., Jr., *Hypersonic and High Temperature Gas Dynamics*, McGraw–Hill, New York, 1989.

[11]Wurster, K. E., Riley, C. J., and Zoby, V., "Engineering Aerothermal Analysis for X-34 Thermal Protection Design," *Journal of Spacecraft and Rockets*, Vol. 36, No. 2, 1999, pp. 216–228; also AIAA Paper 98-0882, Jan. 1998.

[12]Kelly, H. N., and Webb, G. L., "Assessment of Alternate Thermal Protection Systems for the Space Shuttle Orbiter," AIAA Paper 82-0899, June 1982.

[13]Stetson, K. F., "Comments on Hypersonic Boundary-Layer Transition," U.S. Air Force Wright Research and Development Center, WRDC-TR-90-3057, Sept. 1990.

[14]Bouslog, S. A., An, M. Y., and Derry, S. M., "Orbiter Windward Surface Boundary Layer Transition Flight Data," *Orbiter Experiments (OEX) Aerothermodynamics Symposium*, NASA CP-3248, April 1995, pp. 703–739.

[15]Haney, J. W., "Orbiter (Pre STS-1) Aeroheating Design Data Base Development Methodology: Comparison of Wind Tunnel and Flight Test Data," *Orbiter Experiments (OEX) Aerothermodynamics Symposium*, NASA CP-3248, April 1995, pp. 607–675.

[16]Blosser, M. L., "Development of Metallic Thermal Protection Systems for the Reusable Launch Vehicle," NASA TM 110296, Oct. 1996.

[17]Bouslog, S. A., Moore, B., Lawson, I., and Sawyer, J. W., "X-33 Metallic TPS Tests in NASA Langley Research Center High-Temperature Tunnel," AIAA Paper 99-1045, Jan. 1999.

[18]Kontinos, D. A., and Palmer, G., "Numerical Simulation of Metallic Thermal Protection System Panel Bowing," *Journal of Spacecraft and Rockets*, Vol. 36, No. 6, 1999, pp. 842–849.

[19]Berry, S. A., Bouslog, S. A., Brauckmann, G. J., and Caram, J. M., "Shuttle Orbiter Experimental Boundary-Layer Transition Results with Isolated Roughness," *Journal of Spacecraft and Rockets*, Vol. 35, No. 3, 1998, pp. 241–248.

[20]Tribot, J. P., Tran, P., Pallegoix, J. F., Orlowski, M., Bruck, S., Andres, O. P., and Fitzgerald, S. M., "X-38 Aerothermodynamics," Atmospheric Reentry Vehicles and Systems Symposium, Arcachon, France, March 1999.

[21]Berry, S. A., Horvath, T. J., Kowalkowski, M. K., and Liechty, D. S., "X-33 (Rev-F) Aeroheating Results of Test 6770 in NASA Langley 20-Inch Mach 6 Tunnel," NASA TM-1999-209122, March 1999.

[22]Miller, C. G., "Langley Hypersonic Aerodynamic/Aerothermodynamic Testing Capabilities, Present and Future," AIAA Paper 90-1376, June 1990.

[23]Beckwith, I. E., and Miller, C. G., "Aerothermodynamics and Transition in High-Speed Wind Tunnels at NASA Langley," *Annual Review of Fluid Mechanics*, Vol. 22, 1990, pp. 419–439.

[24]Bouslog, S. A., Bertin, J. J., Berry, S. A., and Caram, J. M., "Isolated Roughness Induced Boundary-Layer Transition: Shuttle Orbiter Ground Tests and Flight Experience," AIAA Paper 97-0274, Jan. 1997.

[25]Stainback, P. C., and Kubendran, L. R., "The Measurement of Disturbance Levels in the Langley Research Center 20-Inch Mach 6 Tunnel," NASA CR-4571, March 1994.

[26]Reed, H., Kimmel, R., Arnal, D., and Schneider, S., "Drag Prediction and Transition in Hypersonic Flow," *Sustained Hypersonic Flight*, CP-600, AGARD, Vol. 3, 1997.

[27]Buck, G. M., "Automated Thermal Mapping Techniques Using Chromatic Image Analysis," NASA TM-101554, April 1989.

[28]Buck, G. M., "Surface Temperature/Heat Transfer Measurement Using a Quantitative Phosphor Thermography System," AIAA Paper 91-0064, Jan. 1991.

[29]Berry, S. A., Horvath, T. J., DiFulvio, M., Glass, C., and Merski, N. R., "X-34 Experimental Aeroheating at Mach 6 and 10," AIAA Paper 98-0881, Jan. 1998.

[30]Micol, J. R., "Aerothermodynamic Measurement and Prediction for a Modified Orbiter at Mach 6 and 10 in Air," *Journal of Spacecraft and Rockets*, Vol. 32, No. 5, 1995, pp. 737–748.

[31]Loomis, M. P., Venkatapathy, E., Davies, C. B., Campbell, C. H., Berry, S. A., Horvath, T. J., and Merski, N. R., "Aerothermal Computational Fluid Dynamics Validation and Prediction for the X-38 Program," AIAA Paper 97-2484, June 1997.

[32]Bertin, J. J., Hayden, T. E., and Goodrich, W. D., "Shuttle Boundary-Layer Transition due to Distributed Roughness and Surface Cooling," *Journal of Spacecraft and Rockets*, Vol. 19, No. 5, 1982, pp. 389–396.

[33]Van Driest, E. R., and Blumer, C. B., "Boundary Layer Transition on Cones and Spheres at Supersonic Speeds-Effects of Roughness and Cooling," U.S. Air Force Office of Scientific Research, Rept. 67-2048, July 1967.

[34]Boudreau, A. H., "Artificially Induced Boundary-Layer Transition on Blunt-Slender Cones at Hypersonic Speeds," *Journal of Spacecraft and Rockets*, Vol. 16, No. 4, 1979, pp. 245–251.

[35]Fay, J. A., and Riddell, F. R., "Theory of Stagnation Point Heat Transfer in Dissociated Air," *Journal of Aeronautical Sciences*, Vol. 25, No. 2, 1958, pp. 73–85, 121.

[36]"GASP Version 3, The General Aerodynamic Simulation Program, Computational Flow Analysis Software for the Scientist and Engineer, User's Manual," Aerosoft, Inc., Blacksburg, VA, 1996.

[37]Hamilton, H. H., II, Greene, F. A., DeJarnette, F. R., "Approximate Method for Calculating Heating Rates on Three-Dimensional Vehicles," *Journal of Spacecraft and Rockets*, Vol. 31, No. 3, 1994, pp. 345–354.

[38]Poll, D. I. A., "New Hypothesis for Transition on the Windward Face of the Space Shuttle," *Journal of Spacecraft and Rockets*, Vol. 23, No. 6, 1986, pp. 605–611.

[39]Adams, J. C., Jr., and Martindale, W. R., "Hypersonic Lifting Body Windward Surface Flow-Field Analysis for High Angles of Incidence," Arnold Engineering Development Center-TR-73-2, Feb. 1993.

Color reproductions courtesy of NASA Langley Research Center.